



The potential of wire electron beam additive manufacturing of copper

A. Zamorano Reichold¹ · B. Baufeld¹

Received: 12 May 2023 / Accepted: 10 July 2023 / Published online: 22 November 2023
© The Author(s), under exclusive licence to Springer Nature Switzerland AG 2023

Abstract

Copper presents a number of challenges for additive manufacturing. These include high thermal conductivity, significant light reflectivity, and severe oxide formation. The electron beam as an energy source can overcome these difficulties in the production of copper AM components due to the high power available, the high process energy efficiency, and the fact that the process takes place in vacuum. Non-porous copper components can be produced at high deposition rates of up to 2.5 kg/h using wire electron beam additive manufacturing. This technique can also create multi-material components in both copper and steel, and copper features on copper components. It should be emphasized that an average power of 3.0 kW was sufficient to produce copper features on copper components at the high deposition rate mentioned above. The power and energy distribution of the electron beam can be adjusted at any time. This allows grain growth and the associated microstructure to be influenced. It has been found that using a copper base plate instead of a steel base plate requires significantly different process parameters. Successfully producing geometries on copper base plates is challenging due to the high thermal conductivity of copper and requires a large beam power in the early layers. Pure copper components made by wire electron beam additive manufacturing have an electrical conductivity of 100% of the international standard for annealed copper. By optimizing the energy input and distribution, the ultimate tensile strength of 206 MPa with a strain at failure of 31% can be achieved.

Keywords Additive manufacturing · DED · DED-EB · Copper · Wire

1 Introduction

Copper and copper alloys show for the additive manufacturing (AM) industry the largest annual increase in material consumption at 45%, while the average material consumption of all metal alloys is 32% [1]. Applications for copper products can be found for example in the energy, mobility, and aerospace sectors. These take advantage of the high electrical and thermal conductivity of copper [2]. Additive manufacturing enables complex geometries, thin-walled structures, and new manufacturing possibilities, such as the use of multi-materials [3]. Various additive manufacturing technologies are available for the processing of copper. These are ultrasonic welding, cold spray, binder jetting, metal fused deposition modeling (FDM), laser and electron beam powder bed fusion (PBF-LB, PBF-EB) [1], and directed energy deposition DED [4]. For DED technologies, the thermal energy can be applied by plasma arc

beam (DED-PB), laser beam (DED-LB), or electron beam (DED-EB) [1]. In all three cases, the starting material can be a metal wire, but in the case of DED-LB, powder can also be used as the feedstock [5].

In the case of copper AM, the efficiency of the electron beam is superior to other energy sources. Conventional infrared laser methods have the disadvantage of the high reflectivity of pure copper, up to 96% of the laser power [6]. To overcome this inefficiency, a recent development [7, 8] is the use of green lasers with 45% or blue lasers with 30% reflectivity [5]. In the case of electron beam, the efficiency is much higher since the energy transfers directly from kinetic energy to heat.

While powder bed AM technologies have made significant progress in the development of copper applications, only limited information is available on DED technologies. DED-PB has been experimented with copper alloys. Wang et al. demonstrated the feasibility of processing Cu–Al bronze using this method [9]. However, there is a potential for oxygen contamination during the deposition process of a copper alloy, requiring the use of special inert gas nozzles or chambers [10].

✉ A. Zamorano Reichold
alejandro.zamorano@pro-beam.com

¹ Pro-Beam Additive GmbH, Gilching, Germany

First, DED-LB results for copper components were provided by Siva Prasad et al. [8] where blown powder (99.9% pure copper) and a green laser were applied to achieve a deposition rate of 0.08 kg/hr. They highlighted the significant influence of an oxide skin on the melt pool [8].

For DED-EB, to the authors' knowledge, there are currently only 3 research groups focusing on pure copper [4, 11, 12]. Osipovich et al. [4] used DED-EB with a deposition rate of 1.9 kg/h resulting in small equiaxed grains near the steel baseplate and large columnar grains for higher layers. These columnar grains were elongated along the sample growth direction. They noted that the grain size in the transverse direction exceeded 1 mm, while in the longitudinal direction, it was 7 mm, which was also observed by Panfilov et al. [11] and Baufeld [12]. The mechanical properties in [4] showed anisotropy with ultimate tensile strength (UTS) in the area of pure copper of 180 MPa in horizontal and 125 MPa in vertical direction. Panfilov et al. reported the presence of spherical pores. Due to the elongated grain structure parallel to the deposition direction, a certain degree of anisotropy in the mechanical properties was observed, with a UTS of 138 MPa in the vertical direction and 160 MPa in the horizontal direction [11]. No studies were found in which copper features were built on a copper substrate. Furthermore, Baufeld [12] presented large-scale copper components.

The aim of this paper is to provide further information about the microstructure and properties of copper components built with DED-EB.

2 Experimental methods

2.1 Machine set-up

The components presented in this study were produced using a pro-beam K40 machine equipped with a 4 m³ vacuum chamber, a vertical external static 60 kV electron beam generator, and a fully CNC integrated wire feeder. The

manipulator is capable of linear movement in x, y, and z directions, rotation and tilting. More information about the set-up can be found in [13]. An example of the DED-EB set-up is shown in Fig. 1a, where the wire feeder, the motor, and the gearbox are located in the central box (bright contrast). The wire feed tube and the nozzle extend from this box. The wire used has a 1.2 mm diameter and is either 99.99% pure copper or CuSn1 (material number 2.1006). The components were mounted on S355 steel or copper plates.

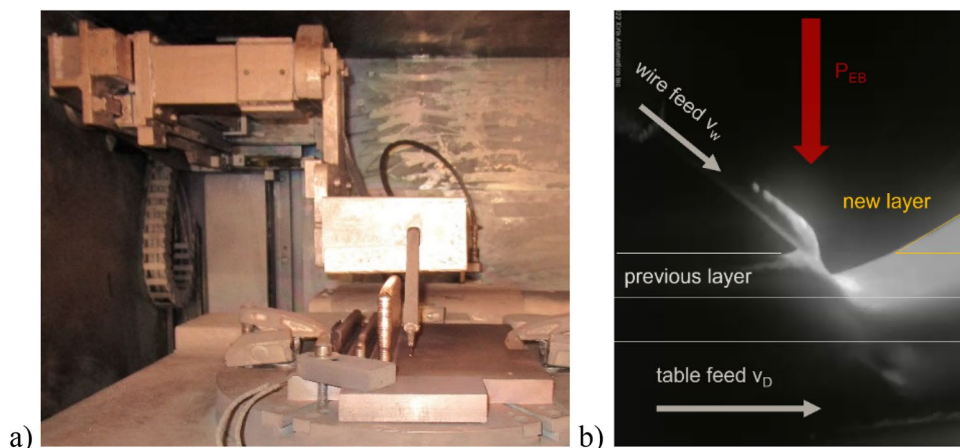
A side view of a running DED-EB process and its schematic description can be seen in Fig. 1b. In this case, the material is deposited with leading wire feed, showing the previous solid layer on the left and the new layer still in liquid form on the right. Ideally, the electron beam creates a melt pool on the substrate or previous layer and melts the wire during deposition, forming a metallic liquid bridge between the melt pool and the wire.

Electromagnetic fields are used to modify the focus length, the beam cross section, and also to rapidly deflect the beam changing the location of beam interaction on the work-piece. As the beam control requires no mechanical movements at all, high-speed beam deflections and thus complex and high-frequency beam patterns are possible, which can be adjusted as required. This enables the beam energy distribution to be manipulated at any time during the process to minimize power consumption.

2.2 Influence on the process parameters

As mentioned before, in the DED-EB process, the electron beam melts the wire and creates a molten pool. The size of the melt pool is determined by the bead width, layer height, and weld penetration depth. The size of the melt pool depends strongly on the beam energy and the different cooling processes used for certain process parameters. For the first layers, the dominant cooling process is conduction cooling. As the number of layers increases, the influence of conduction cooling decreases and the dominant cooling

Fig. 1 **a** Overview of the DED-EB set-up with several walls **b** Side view of the DED-EB process with a vertical electron beam PEB © All rights reserved



process is radiation cooling (since convection cooling does not occur in high vacuum). This change in the dominant cooling processes means that the magnitude and distribution of the beam energy must be adjusted with the height (Fig. 2).

The material and the geometry of the base plate determine the conduction cooling. In the case of copper, the thermal conductivity is over two times bigger than the one of steel. As a result, when using a copper base plate, a significantly higher beam power is required for the first layers (Fig. 2) to achieve sufficient weld penetration depth and the related bond between the substrate and AM component.

Parameter set 1 was optimized for base plate A, resulting in a cylinder with the desired geometry (Fig. 3a). For the larger base plate geometry B, with the same parameter set 1, insufficient beam power was provided due to the higher cooling power, resulting in poorer sample geometry (Fig. 3b). It can clearly be seen in Fig. 3b that the power applied in the first layers was sufficient to produce a good bond between the base plate and the AM component. However, the power reduction of parameter set 1 is too high as the previously built layers cool down much faster than in the cylinder in Fig. 3a. Therefore, from layer 4 onwards, there is not enough power available to melt the layer below. With parameter set 2, about twice the beam power toward the end of the set-up as parameter set 1, for base plate geometry B, a good cylinder with straight walls was obtained (Fig. 3d). On the other hand, parameter set 2 leads to excessive overheating for base plate geometry A (Fig. 3c).

2.3 Microstructure and material properties

From previous studies, it is known that epitaxial grain growth occurs during the process, resulting in long vertical grains [4, 11, 12]. Here, two pure copper walls and two cylinders are compared, each with different process parameters,

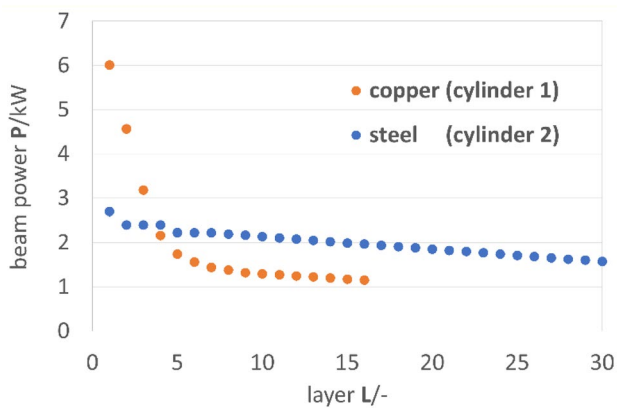


Fig. 2 Beam power plotted over layer number for cylinders build on a copper (cylinder 1) and a steel base plate (cylinder 2) © All rights reserved

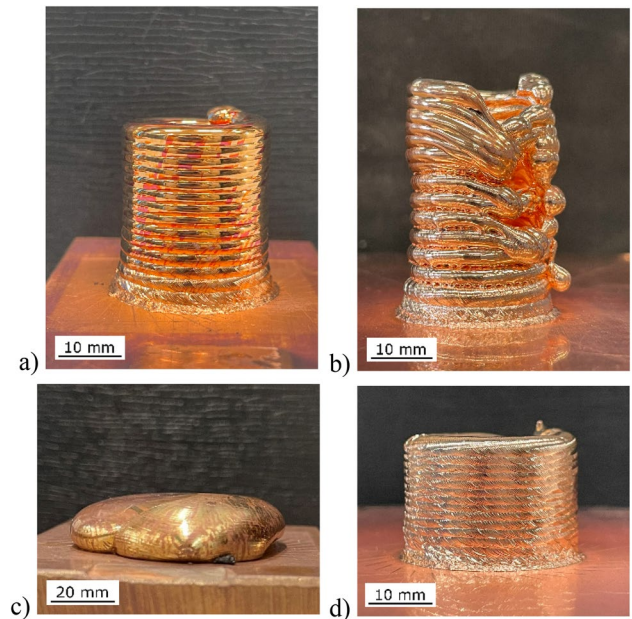


Fig. 3 Pure copper cylinders built with parameter set 1 (a, b) and parameter set 2 (c, d) for base plate geometry A (a, c) and base plate geometry B (b, d) © All rights reserved

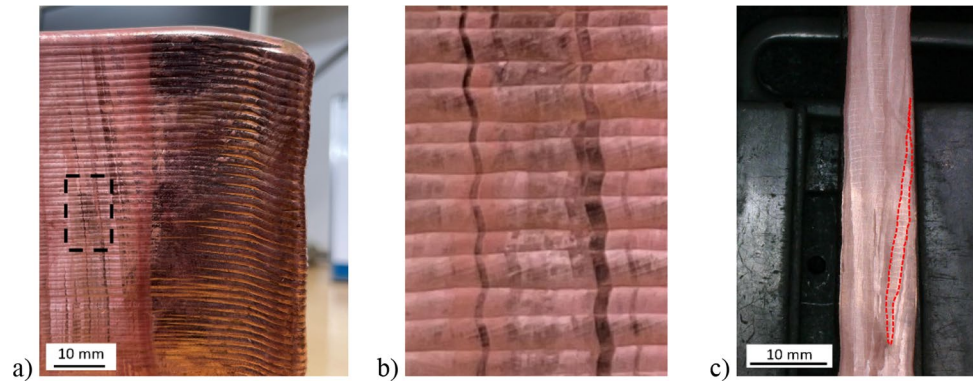
as shown in Table 1. A pro-beam proprietary beam deflection (beam pattern) was used for all components.

Wall 1 was built with a deposition rate of $\dot{m} = 2.0\text{kg/h}$, an averaged power of $P = 3.7\text{kW}$ and an averaged energy input per unit length of $E = 0.43\text{kJ/mm}$. The wall was built by alternating trailing and leading wire feed. Figure 4a gives a view on the side of the wall, where long grains of copper, up to 30 mm in length can be seen. A closer look at the Fig. 4b reveals that the elongated grains extend almost vertically over many layers, but the preferred growth direction

Table 1 Substrate material, process parameters and final dimensions for walls 1 & 2 and cylinders 1 & 2

Attribute	Unit	Wall 1	Wall 2	Cylinder 1	Cylinder 2
Substrate material		Copper	Copper	Copper	Steel
Acceleration voltage	kV	60	60	60	60
Energy input per unit length	kJ/mm	<0.47	<1.4	<1	<0.16
Wire feed rate	m/min	3	4	3	3
Feed angle	°	~30	~30	~30	~30
Wire tip length	mm	13	13	13	13
Layer idle time	s	30	40	–	–
Final product height	mm	78	86	29	22
Wall width	mm	~9	~8	4	4
Outer diameter	mm	–	–	22	22
Mean layer height	mm	1	2	2	2

Fig. 4 Pure copper wall 1 with an average beam power of 3.7 kW built on a copper substrate (a) longitudinal side view (dotted rectangle indicates detailed area of (b) detailed longitudinal side view (c) cross section © All rights reserved



changes slightly layer by layer, resulting in “zig-zag” grains. This is probably due to the layer-by-layer change in direction of the temperature gradient caused by the alternating layer build-up direction. Osipovich et al. [4] reported also “zig-zag” grain pattern. Despite this change in growth direction, epitaxial growth occurs maintaining the crystal orientation. The cross section of this copper wall exhibits clearly these elongated grains which slightly tilt from center toward the surface of the wall (Fig. 4c).

Figure 5 shows the copper wall 2 built also with alternating and trailing wire on a copper substrate, however with the difference that a lower average beam power $P = 3.0\text{ kW}$ was applied at a higher deposition rate $\dot{m} = 2.6\text{ kg/h}$. To achieve approximately the same wall width as for wall 1 (Fig. 4), the average energy input per unit length was increased to $E = 0.67\text{ kJ/mm}$ by reducing the welding speed. This resulted in a change of the grain growth behavior (Fig. 5). Figure 5a, b shows that thin grains extend in an angle over many layers, while the cross sections of the wall 2 (Fig. 5c) reveal significantly smaller structures. Compared to Fig. 4b, the grains of wall 2 (Fig. 5b) grow more inclined. Likewise, the change in direction after each layer is stronger and thus the angle of the grain preference growth direction is smaller than in wall 1 (Fig. 4b). Due to the more tilted growth of the grains in wall 2 (Fig. 5b), more grains are cut in the cross

section and the grains appear to be smaller (Fig. 5c). Horizontal liquidus lines [12] are visible in both walls (Fig. 4c and Fig. 5b, c). It is noteworthy that in Fig. 5b the horizontal liquidus lines lie at the reversal point of the grain growth direction supporting the assignment of these lines as liquidus lines.

As mentioned above, investigations of copper cylinders on a copper (cylinder 1) and steel substrate (cylinder 2) were carried out (Fig. 6), using the beam power as indicated in Fig. 2 (further process parameter see Table 1). Figure 6a demonstrates the high quality of the interface between copper AM component and the substrate. The grains appear in cross section equiaxed and the grain size increases with built height.

Figure 6b illustrates cylinder 2 with a steel substrate. Here, there was a considerable weld penetration and material intermixing, up to a few layers high into the AM copper component. Near the bottom, the copper grains are much smaller and more equiaxed (Fig. 6b). At approximately 5 mm build-up height, the epitaxial grain growth begins. This change in grain size was also observed in [4]. In the case of the cylinder 1 built on a copper plate (Fig. 6a), the elongated grains are significantly smaller than in the case of the cylinder 2 built on steel (Fig. 6b). This may be due to the higher thermal conductivity of the copper base plate,

Fig. 5 Pure copper wall 2 with an average beam power of 3.0 kW built on a copper substrate (a) side view on the wall (b) detailed length section (c) cross section © All rights reserved

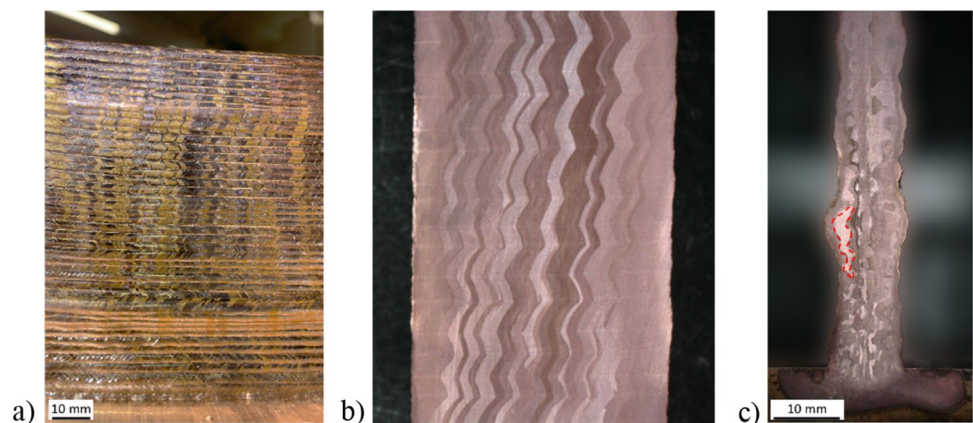


Fig. 6 Sections of pure copper cylinders on (a) a copper base plate (cylinder 1) and (b) a steel base plate (cylinder 2) © All rights reserved

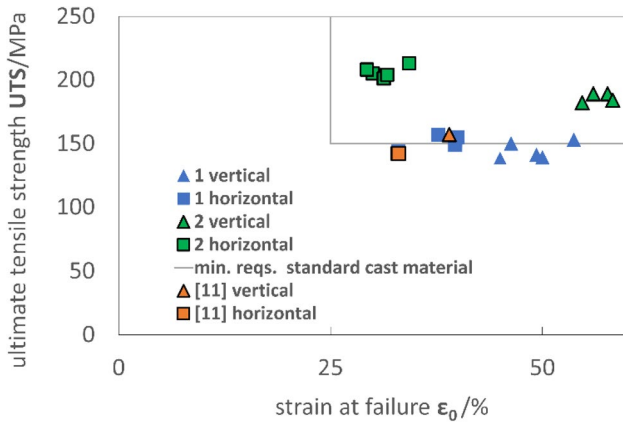
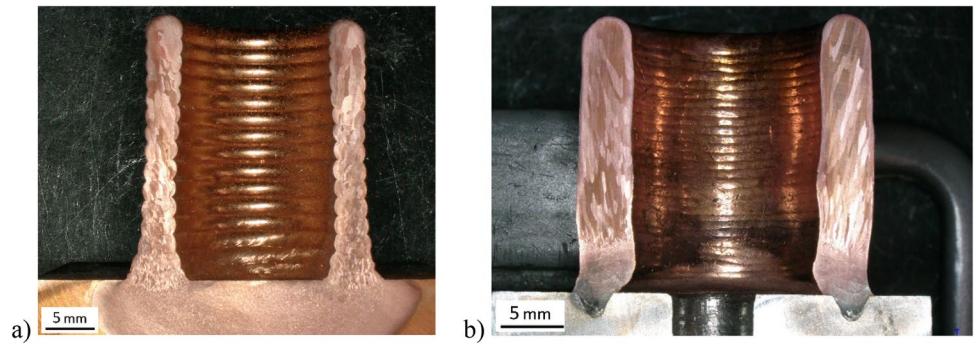


Fig. 7 UTS over strain at failure for horizontal and vertical specimens extracted from wall 1 and 2 (blue and green) built on copper plates and literature values (orange) [11]; Min. requirements for cast material CC040A (EN 1982: 2008) indicated by solid lines © All rights reserved

but also to the optimized energy input and distribution. This lower energy input, shown in Fig. 2, leads to higher track heights resulting in a more pronounced grooved surface.

The results of tensile testing of round specimen (DIN EN ISO 6892–1) derived from the copper walls 1 and 2 are summarized in Fig. 7 with specimens extracted horizontally

and vertically from the walls. The average ultimate tensile strength (UTS) of copper wall 1 specimen in horizontal direction ($UTS_{\varnothing h1} = 152\text{MPa}$) is slightly larger than in vertical direction ($UTS_{\varnothing v1} = 143\text{MPa}$). The strain at failure for horizontal direction ($\epsilon_{0,\varnothing h1} = 38\%$) is smaller than in vertical direction ($\epsilon_{0,\varnothing v1} = 49\%$). Generally, for wall 2, the UTS is significantly higher than for wall 1. In horizontal direction, the average $UTS_{\varnothing h2}$ was 206 MPa (36% higher than for wall 1) with an average strain at failure of $\epsilon_{0,\varnothing h2} = 31\%$, and in vertical direction 186 MPa (30% higher than for wall 1) with an average strain at failure of $\epsilon_{0,\varnothing v2} = 57\%$. Panfilov et al. [11] have reported similar results as in the present work for wall 1. Osipovich showed for the areas of pure copper a UTS of 125 MPa in vertical and 180 MPa in horizontal direction [4]. The increase in UTS of wall 2 compared to wall 1 is probably related to the significant change in grain structure. The high strain at failure indicates a high degree of plastic deformation.

The electrical conductivity of a copper wall was measured with the phase sensitive eddy current method using a SIGMASCOP SMP350 (Helmut Fischer GmbH). Regardless of the orientation, the result was $(57.8 \pm 0.6)\text{MS/m}$. This corresponds to 99.7% of the international annealed copper standard (IACS) and is equivalent to an electrical resistivity of $\rho = 0.0173\ \Omega\text{mm}^2/\text{m}$. This excellent conductivity indicates its high quality and absence of significant defects.

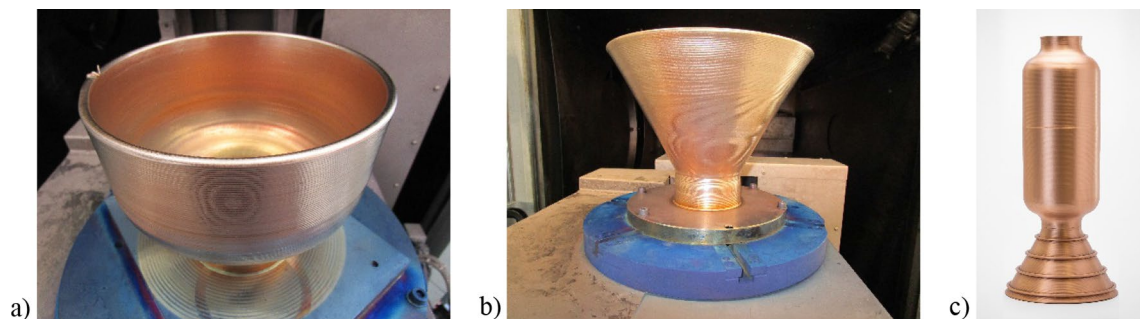


Fig. 8 Axially symmetrical CuSn1 components (as built, no surface machining or cleaning). a: Half shell, b: Cone, c: Model of a rocket motor joined by electron beam welding © All rights reserved

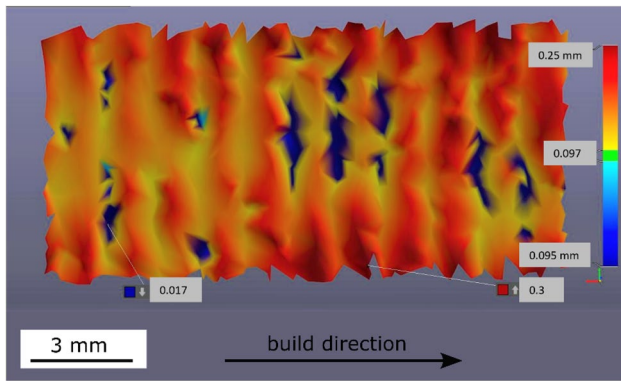


Fig. 9 Color map of the inner surface to demonstrate the surface profile, covering 11 layers in the center of the cone, derived from a 3D laser scan © All rights reserved

3 Case studies

3.1 Model of a rocket motor

To illustrate the applicability of DED-EB for copper components, a model of a CuSn1 rocket motor was built. Two half shells (Fig. 8a) and a cone (Fig. 8b) were separately manufactured. In addition, the cone received four rings

by DED-EB. The net production time for these three parts (without handling, evacuation, and cooling) was 12 h.

A remarkably smooth surface quality was achieved without any cracks or defects in the components. It should be highlighted that the components in Fig. 8a and b are in the as-built state without any surface machining or cleaning. Figure 9 shows the inner surface of a cone determined by a 3D laser scan. A color map is used to highlight the extent of the waviness. The wavelength is 1.4 mm, and the wave amplitude is about 0.03 mm.

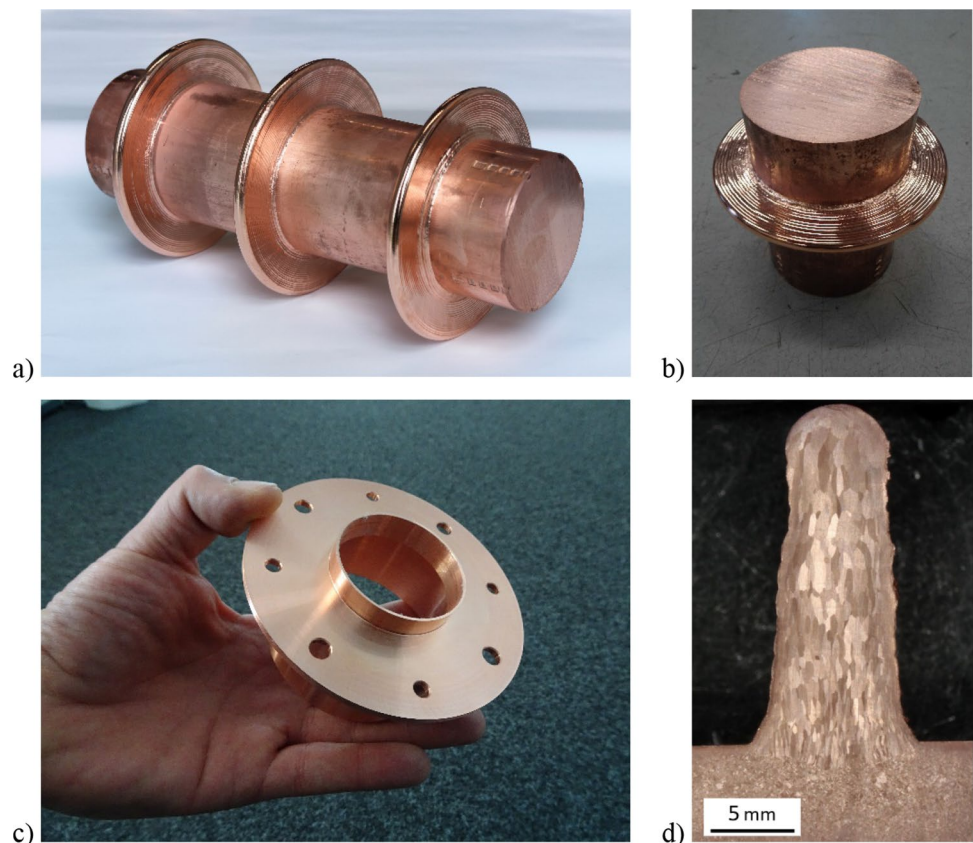
The three components were joined together by electron beam welding. The result is a 22 kg model of a rocket motor with a height of 650 mm and a maximum diameter of 295 mm (Fig. 8c).

3.2 High frequency conductor

For a series of plasma-activated chemical vapor deposition (CVD) systems, a customer required high-frequency conductors (Fig. 10c). The solution that met this requirement is a good example of intelligent AM, taking into account the tension between the cost of the material, of the AM process and of the finishing, and the availability of the raw material.

Manufacturing the product entirely by AM would mean the lowest material and machining costs, but the highest

Fig. 10 Serial production of a high-frequency copper conductor. **a** Three rings of pure copper on a rod. **b** Cut component. **c** Finished component after machining. **d** Radial section through the semi-finished AM component © All rights reserved



process costs. Therefore, a semi-finished product with a geometry very close to that of the final product is a good choice if available. This semi-finished product becomes part of the final component and only a minimal amount of AM needs to be performed. This approach can be a cheaper and faster way to manufacture the product.

In the case of this study, the raw material was not readily available to machine the entire component from the solid. In addition, this traditional approach would also involve a significant amount of machining and material waste. Therefore, a copper rod with a diameter of 80 mm was used as the starting material and rings of pure copper were applied using DED-EB (Fig. 10a). The production of each ring took 14 min. The parts were then cut (Fig. 10b) and machined (Fig. 10c). The finished part has an outer diameter of 120 mm with no visible defects at the interface or in the AM part. Figure 10d shows the radial section through the AM component. The copper AM component is excellently bonded to the copper cylinder.

4 Conclusions

This work has shown that DED-EB is a competitive AM technology for creating defect-free copper components with excellent surface quality on copper or steel substrates at high deposition rates. It was shown that the microstructure and the material properties can be influenced by optimizing the energy input and energy distribution. Tensile strength up to 206 MPa and strain at failure up to 57% were realized. Electrical conductivities of 98% IACS were obtained. Further work will be dedicated on increasing the deposition rate. First preliminary results already indicate the potential to deposit at 7.5 kg/h.

Funding This study was funded by pro-beam additive GmbH.

Declarations

Conflict of interest The authors are employed by pro-beam additive GmbH by the time of the study.

References

1. AMPower (2022) Study on Copper Additive Manufacturing: A technology study on the status quo of copper in AM.
2. Jiang Q, Zhang P, Yu Z et al (2021) A review on additive manufacturing of pure copper. *Coatings* 11:740. <https://doi.org/10.3390/coatings11060740>
3. Paul R, Gradl, Dr. Christopher S, Protzb, Dr. David L, Ellisc et al. Progress in Additively Manufactured Copper-Alloy GRCop-84, GRCop-42, and Bimetallic Combustion Chambers for Liquid Rocket Engines. In: 70th International Astronautical Congress (IAC)
4. Osipovich K, Vorontsov A, Chumaevskii A et al (2022) Features of microstructure and texture formation of large-sized blocks of C11000 copper produced by electron beam wire-feed additive technology. *Materials* (Basel). <https://doi.org/10.3390/ma15030814>
5. ISO ISO/ASTM 52900:2015: Additive manufacturing — General principles — Terminology
6. Bowmun R.L., Jack J.R., Spisz E.W. et al. (1969) Solar absorptances and spectral reflectances of 12 metals for temperatures ranging from 300 to 500 K. Other - NASA Technical Note (TN)
7. Hori E, Sato Y, Shibata T et al (2021) Development of SLM process using 200 W blue diode laser for pure copper additive manufacturing of high density structure. *J Laser Appl* 33:12008. <https://doi.org/10.2351/7.0000311>
8. Siva Prasad H, Brueckner F, Volpp J et al (2020) Laser metal deposition of copper on diverse metals using green laser sources. *Int J Adv Manuf Technol* 107:1559–1568. <https://doi.org/10.1007/s00170-020-05117-z>
9. Wang Y, Chen X, Konovalov S et al (2019) In-situ wire-feed additive manufacturing of Cu-Al alloy by addition of silicon. *Appl Surf Sci* 487:1366–1375. <https://doi.org/10.1016/j.apsusc.2019.05.068>
10. Dong B, Pan Z, Shen C et al (2017) Fabrication of copper-rich Cu-Al alloy using the wire-arc additive manufacturing process. *Metall and Materi Trans B* 48:3143–3151. <https://doi.org/10.1007/s11663-017-1071-0>
11. Panfilov A, Knyazhev E, Kalashnikova T et al (2020) Deformation uniformity of additively manufactured materials on the example of austenitic stainless steel 321 and copper C11000. *J Phys Conf Ser*. <https://doi.org/10.1088/1742-6596/1611/1/012005>
12. Baufeld B (2023) Wire electron beam additive manufacturing of copper. In *J Phys Conf Ser*. <https://doi.org/10.1088/1742-6596/2443/1/012001>
13. Baufeld B., Schönfelder S., Löwer T. (2021) Wire electron beam additive manufacturing at pro-beam. In: IEBW - International Electron Beam Welding Conference 2021

Publisher's Note Springer Nature remains neutral with regard to jurisdictional claims in published maps and institutional affiliations.

Springer Nature or its licensor (e.g. a society or other partner) holds exclusive rights to this article under a publishing agreement with the author(s) or other rightsholder(s); author self-archiving of the accepted manuscript version of this article is solely governed by the terms of such publishing agreement and applicable law.